nature

https://doi.org/10.1038/s41586-020-2358-x

Supplementary information

Integrated turnkey soliton microcombs

In the format provided by the authors and unedited

Boqiang Shen, Lin Chang✉, Junqiu Liu, Heming Wang, Qi-Fan Yang, Chao Xiang, Rui Ning Wang, Jijun He, Tianyi Liu, Weiqiang Xie, Joel Guo, David Kinghorn, Lue Wu, Qing-Xin Ji, Tobias J. Kippenberg✉, Kerry Vahala✉ & John E. Bowers

Integrated turnkey soliton microcombs: Supplementary Information

Boqiang Shen[1,†], Lin Chang[2,†,*], Junqiu Liu[3,†], Heming Wang[1,†], Qi-Fan Yang[1,†], Chao Xiang[2], Rui Ning Wang[3], Jijun He[3], Tianyi Liu[3], Weiqiang Xie[2], Joel Guo[2], David Kinghorn[2,4], Lue Wu[1], Qing-Xin Ji[1,5], Tobias J. Kippenberg[3,*], Kerry Vahala[1,*] and John E. Bowers[2]

[1]T. J. Watson Laboratory of Applied Physics, California Institute of Technology, Pasadena, CA 91125, USA

[2]ECE Department, University of California Santa Barbara, Santa Barbara, CA 93106, USA

[3]Institute of Physics, Swiss Federal Institute of Technology Lausanne (EPFL), CH-1015 Lausanne, Switzerland

[4]Pro Precision Process & Reliability, LLC, Carpinteria, CA 93014, USA

[5]School of Physics, Peking University, Beijing 100871, China

[†]These authors contributed equally to this work.

[*]Corresponding authors: linchang@ucsb.edu, tobias.kippenberg@epfl.ch, vahala@caltech.edu

I. THEORY OF TURNKEY SOLITON GENERATION

The injection locking system consists of three parts: the soliton optical field A_{S}, the backscattering field A_{B}, and the laser field A_{L}. The complete equations of motions are[1,2]:

$$\begin{aligned}
\frac{\partial A_{\mathrm{S}}}{\partial t} &= -\frac{\kappa}{2}A_{\mathrm{S}} - i\delta\omega A_{\mathrm{S}} + i\frac{D_2}{2}\frac{\partial^2 A_{\mathrm{S}}}{\partial\theta^2} + i\frac{\kappa}{2}\frac{|A_{\mathrm{S}}|^2+2|A_{\mathrm{B}}|^2}{E_{\mathrm{th}}}A_{\mathrm{S}} + i\beta^*\frac{\kappa}{2}A_{\mathrm{B}} - \sqrt{\kappa_{\mathrm{R}}\kappa_{\mathrm{L}}}e^{i\phi_{\mathrm{B}}}A_{\mathrm{L}} \\
\frac{dA_{\mathrm{B}}}{dt} &= -\frac{\kappa}{2}A_{\mathrm{B}} - i\delta\omega A_{\mathrm{B}} + i\frac{\kappa}{2}\frac{|A_{\mathrm{B}}|^2+2\int_0^{2\pi}|A_{\mathrm{S}}|^2 d\theta/(2\pi)}{E_{\mathrm{th}}}A_{\mathrm{B}} + i\beta\frac{\kappa}{2}\overline{A_{\mathrm{S}}} \\
\frac{dA_{\mathrm{L}}}{dt} &= i(\delta\omega_{\mathrm{L}}-\delta\omega)A_{\mathrm{L}} - \frac{\gamma}{2}A_{\mathrm{L}} + \frac{g(|A_{\mathrm{L}}|^2)}{2}(1+i\alpha_g)A_{\mathrm{L}} - \sqrt{\kappa_{\mathrm{R}}\kappa_{\mathrm{L}}}e^{i\phi_{\mathrm{B}}}A_{\mathrm{B}}
\end{aligned} \tag{S1}$$

where the field amplitudes are normalized so that $\int_0^{2\pi}|A_{\mathrm{S}}|^2 d\theta/(2\pi)$, $|A_{\mathrm{B}}|^2$ and $|A_{\mathrm{L}}|^2$ are the optical energies of their respective fields, t is the evolution time, θ is the resonator angular coordinate, κ is the resonator mode loss rate (assumed to be equal for A_{S} and A_{B}), $\delta\omega$ is the detuning of the cold-cavity resonance compared to injection-locked laser ($\delta\omega > 0$ indicates red detuning of the pump frequency relative to the cavity frequency), D_2 is the second-order dispersion parameter, E_{th} is the parametric oscillation threshold for intracavity energy, β is the dimensionless backscattering coefficient (normalized to $\kappa/2$), ϕ_{B} is the propagation phase delay between the resonator and the laser, κ_{R} and κ_{L} are the external coupling rates for the resonator and laser respectively, $\delta\omega_{\mathrm{L}}$ is the detuning of the cold-cavity resonance relative to the cold laser frequency, γ is the laser mode loss rate, $g(|A_{\mathrm{L}}|^2) \equiv g_0/(1+|A_{\mathrm{L}}|^2/|A_{\mathrm{L,sat}}|^2)$ is the intensity-dependent gain, g_0 is the gain coefficient, $|A_{\mathrm{L,sat}}|^2$ is the saturation energy level, and α_g is the amplitude-phase coupling factor. The average soliton field amplitude $\overline{A_{\mathrm{S}}} = \int_0^{2\pi} A_{\mathrm{S}} d\theta/(2\pi)$ is also the amplitude on the pumped mode, and by using $\overline{A_{\mathrm{S}}}$ in the equation for A_{B} we have assumed that only the mode being pumped contributes significantly in the locking process, which can be justified if a single-frequency laser is used. We note that the equations are effectively referenced to the frequency of the injection-locked laser instead of the free-running laser, which will simplify the following discussions. The frequency difference between the cold laser and the injection-locked laser is given by $\delta\omega - \delta\omega_{\mathrm{L}}$.

We will introduce some other dimensionless quantities to facilitate the discussion. Define: normalized soliton field amplitude as $\psi = A_{\mathrm{S}}/\sqrt{E_{\mathrm{th}}}$, normalized total intracavity power as $P = \int_0^{2\pi}|A_{\mathrm{S}}|^2 d\theta/(2\pi E_{\mathrm{th}})$, normalized amplitude on the pump, backscattering and laser mode as $\rho = \overline{A_{\mathrm{S}}}/\sqrt{E_{\mathrm{th}}}$, $\rho_{\mathrm{B}} = A_{\mathrm{B}}/\sqrt{E_{\mathrm{th}}}$, $\rho_{\mathrm{L}} = A_{\mathrm{L}}/\sqrt{E_{\mathrm{th}}}$ respectively, normalized detuning of cavity as $\alpha = 2\delta\omega/\kappa$, and normalized evolution time as $\tau = \kappa t/2$. The equation for A_{S} and A_{B} can then be put into the dimensionless form

$$\begin{aligned}
\frac{\partial\psi}{\partial\tau} &= -(1+i\alpha)\psi + i\frac{D_2}{\kappa}\frac{\partial^2\psi}{\partial\theta^2} + i(|\psi|^2+2|\rho_{\mathrm{B}}|^2)\psi + i\beta^*\rho_{\mathrm{B}} - \frac{2\sqrt{\kappa_{\mathrm{R}}\kappa_{\mathrm{L}}}}{\kappa}e^{i\phi_{\mathrm{B}}}\rho_{\mathrm{L}} \\
\frac{d\rho_{\mathrm{B}}}{d\tau} &= -(1+i\alpha)\rho_{\mathrm{B}} + i(2P+|\rho_{\mathrm{B}}|^2)\rho_{\mathrm{B}} + i\beta\rho
\end{aligned} \tag{S2}$$

The laser dynamics for A_L are split into amplitude and phase parts:

$$\frac{1}{|A_\mathrm{L}|}\frac{d|A_\mathrm{L}|}{dt} = -\frac{\gamma}{2} + \frac{g(|A_\mathrm{L}|^2)}{2} - \mathrm{Re}\left[\sqrt{\kappa_\mathrm{R}\kappa_\mathrm{L}}e^{i\phi_\mathrm{B}}\frac{A_\mathrm{B}}{A_\mathrm{L}}\right]$$
$$\frac{d\phi_\mathrm{L}}{dt} = \delta\omega_\mathrm{L} - \delta\omega + \frac{g(|A_\mathrm{L}|^2)}{2}\alpha_g - \mathrm{Im}\left[\sqrt{\kappa_\mathrm{R}\kappa_\mathrm{L}}e^{i\phi_\mathrm{B}}\frac{A_\mathrm{B}}{A_\mathrm{L}}\right]$$

where Re[·] and Im[·] are the real and imaginary part functions, respectively. The laser power without backscatter feedback $|A_\mathrm{L}^{(0)}|$ satisfies $g(|A_\mathrm{L}^{(0)}|^2) = \gamma$. Expanding the gain around this point gives

$$\frac{1}{|A_\mathrm{L}|}\frac{d|A_\mathrm{L}|}{dt} = -g'\frac{|A_\mathrm{L}|^2 - |A_\mathrm{L}^{(0)}|^2}{|A_\mathrm{L,sat}|^2} - \mathrm{Re}\left[\sqrt{\kappa_\mathrm{R}\kappa_\mathrm{L}}e^{i\phi_\mathrm{B}}\frac{A_\mathrm{B}}{A_\mathrm{L}}\right]$$

where $g' = g_0/(1+|A_\mathrm{L}^{(0)}|^2/|A_\mathrm{L,sat}|^2)^2$ is the gain derivative that represents the relaxation rate of the gain dynamics. Typical values for g' are on the order of several GHz for III-V semiconductor lasers, which is much faster compared to the resonator dynamics. Accordingly, the laser amplitude can be adiabatically eliminated (i.e., assume $d|A_\mathrm{L}|/dt = 0$) so that the laser power adiabatically tracks the feedback. The gain can be solved as,

$$\frac{g(|A_\mathrm{L}|^2)}{2} = \frac{\gamma}{2} + \mathrm{Re}\left[\sqrt{\kappa_\mathrm{R}\kappa_\mathrm{L}}e^{i\phi_\mathrm{B}}\frac{A_\mathrm{B}}{A_\mathrm{L}}\right]$$

which, under the assumption of fast relaxation rates, becomes independent of the specific details of gain. Substituting this equation into the phase equation and normalizing results in an Adler-like equation:

$$\frac{d\phi_\mathrm{L}}{d\tau} = \alpha_\mathrm{L} - \alpha - \mathrm{Im}\left[\frac{2\sqrt{\kappa_\mathrm{R}\kappa_\mathrm{L}}}{\kappa}(1-i\alpha_g)e^{i\phi_\mathrm{B}}\frac{\rho_\mathrm{B}}{\rho_\mathrm{L}}\right] \tag{S3}$$

where $\alpha_\mathrm{L} = (2\delta\omega_\mathrm{L} + \alpha_g\gamma)/\kappa$ is the normalized detuning of the cold-cavity resonance compared to the free-running hot laser.

To simplify the equations further we also consider the following approximation for the propagation phase ϕ_B, which depends on the precise frequency of the locked laser and material dispersion. We assume that the feedback length is short ($L \ll c/(n\kappa)$, where c is the speed of light in vacuum and n is the refractive index of the material) so that ϕ_B can be treated as constant. This approximation is equivalent to assuming that the free spectral range (FSR) of a cavity equal in length to the feedback path is much larger than the linewidth of the high-Q resonator. By defining a pump phase variable $z = -e^{i\phi_\mathrm{B}}e^{i\phi_\mathrm{L}}$, the equations can be written as

$$\begin{aligned}
\frac{\partial\psi}{\partial\tau} &= -(1+i\alpha)\psi + i\frac{D_2}{\kappa}\frac{\partial^2\psi}{\partial\theta^2} + i(|\psi|^2 + 2|\rho_\mathrm{B}|^2)\psi + i\beta^*\rho_\mathrm{B} + zF \\
\frac{d\rho_\mathrm{B}}{d\tau} &= -(1+i\alpha - 2iP - i|\rho_\mathrm{B}|^2)\rho_\mathrm{B} + i\beta\rho \\
\frac{1}{iz}\frac{dz}{d\tau} &= \alpha_\mathrm{L} - \alpha + K\mathrm{Im}\left[e^{i\phi}\frac{\rho_\mathrm{B}}{i\beta z F}\right], \quad |z| = 1
\end{aligned} \tag{S4}$$

where we defined: the normalized pump,

$$F = \frac{2\sqrt{\kappa_\mathrm{R}\kappa_\mathrm{L}}}{\kappa}|\rho_\mathrm{L}| \tag{S5}$$

the locking bandwidth,

$$K = \frac{4\kappa_\mathrm{R}\kappa_\mathrm{L}}{\kappa^2}|\beta|\sqrt{1+\alpha_g^2} \tag{S6}$$

and the feedback phase,

$$\phi = 2\phi_\mathrm{B} - \arctan(\alpha_g) + \mathrm{Arg}[\beta] + \frac{\pi}{2} \tag{S7}$$

where Arg[·] is the argument function. The feedback phase ϕ contains phase contributions from the propagation length, the amplitude-phase coupling, the backscattering, as well as an extra $\pi/2$ added to the definition of ϕ such that the mode is locked to the centre at $\phi = 0$ (as discussed below).

We note that the feedback fields considered in Eq. (S4) come entirely from inside the resonator. In experiments, defects and facets of the coupling waveguide can also induce reflections. However, these are neglected in the injection locking dynamics by the following arguments. Multiple reflection sources can be incorporated into Eq. (S4) by adding a feedback term corresponding to each source. However, the cumulative effect of such reflections will be to produce a wavelength dependence that is weak compared to the resonator mode, which is spectrally very narrow on account of its high optical Q. Such a weak wavelength dependence means that these fields do not contribute to the locking (i.e., a constant term is added to the phasor equation in Eq. (S4), which can then be absorbed into the free-running laser frequency). As a specific illustration of this idea, consider that the facet reflections at the end of the waveguide form a kind of Fabry-Perot resonator. However, the Q of its resonances will be quite low and accordingly the linewidth will be of order the FSR associated with the waveguide length. Moreover, this FSR is also comparable in scale to the FSR of the high-Q resonator, the resonances of which are many orders narrower than the resonator FSR. As a result, any wavelength dependence introduced by reflections in the waveguide will be spectrally slow in comparison to those introduced by the resonator.

For stationary solutions (e.g., a stable soliton), when backscattering is weak ($\beta \ll 1$) so that nonlinearities caused by $|\rho_\mathrm{B}|^2$ in Eq. (S2) are negligible in comparison to the soliton driven nonlinear terms, ρ_B can be found as

$$\rho_\mathrm{B} = \frac{i\beta\rho}{1+i(\alpha-2P)} \tag{S8}$$

and the laser phasor equation reduces to an algebraic equation for the detuning α,

$$\alpha = \alpha_\mathrm{L} + K\mathrm{Im}\left[e^{i\phi}\frac{1}{1+i(\alpha-2P)}\frac{\rho}{zF}\right] \tag{S9}$$

Finally, neglecting the small coupled amplitude from ρ_B to ψ, the equation for the soliton field reads

$$-(1+i\alpha)\psi + i\frac{D_2}{\kappa}\frac{\partial^2\psi}{\partial\theta^2} + i|\psi|^2\psi + zF = 0 \tag{S10}$$

We have therefore recovered a conventional Lugiato-Lefever equation, with an additional equation that describes the detuning determined by injection locking. This shows that the spectral properties of the injection-locked solitons are not much different from a conventional soliton. The main difference is the comb formation dynamics.

It is known that combs and solitons will emerge from a continuous-wave (CW) background when its power exceeds the parametric oscillation threshold ($|\rho| > 1$), and it is desirable to first study the CW excitation of the system by setting $D_2 = 0$. In this case, the Lugiato-Lefever partial differential equation reduces to an ordinary differential equation with $\psi = \rho$ and $P = |\rho|^2$. The steady state solution can be found from

$$zF = [1 + i(\alpha - |\rho|^2)]\rho \tag{S11}$$

and the locking equilibrium reduces to

$$\alpha = \alpha_\mathrm{L} + K\mathrm{Im}\left[e^{i\phi}\frac{1}{1+i(\alpha-2P)}\frac{1}{1+i(\alpha-P)}\right] = \alpha_\mathrm{L} + K\chi(P,\alpha,\phi) \tag{S12}$$

where we have defined the CW locking response function:

$$\chi(P,\alpha,\phi) = \frac{(3P-2\alpha)\cos\phi + (1-2P^2+3P\alpha-\alpha^2)\sin\phi}{[1+(\alpha-P)^2][1+(\alpha-2P)^2]} \tag{S13}$$

To obtain analytical results, we will also make the approximation of infinite locking bandwidth limit (i.e., $K \to \infty$), which makes the detuning independent of the free-running laser frequency. The locking condition is then equivalent to setting the locking response function to zero:

$$(3P-2\alpha)\cos\phi + (1-2P^2+3P\alpha-\alpha^2)\sin\phi = 0 \tag{S14}$$

Fig. S1 shows a plot for Eq. (S11) with different pumping powers $|F|^2$ and Eq. (S14) with different feedback phases ϕ. The intersecting point of the two curves gives the CW steady state of the cavity. Note that there are two solutions to the quadratic equation Eq. (S14). Only the solution branch that satisfies $\partial\chi/\partial\alpha < 0$ is plotted, which are the stable locking solutions (stable in the sense of CW excitations; the instability arising from modulations are considered below). The opposite case $\partial\chi/\partial\alpha > 0$ drives the frequency away from the equilibrium.

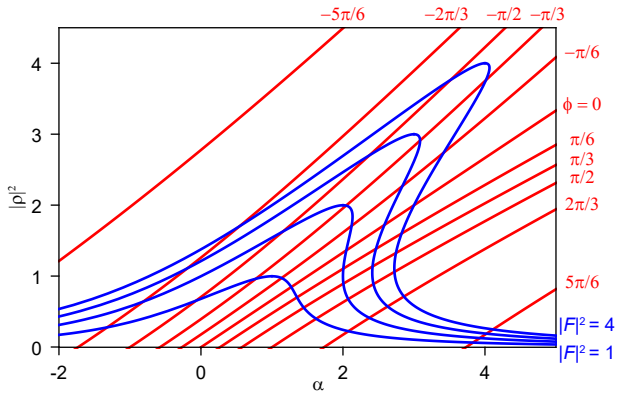

Fig. S1: **Continuous-wave states of the injection-locked nonlinear resonator.** Horizontal axis is the normalized detuning α, and vertical axis is the normalized optical energy on the pump mode $|\rho|^2$. Resonator characteristics are shown as the blue curves, with $|F|^2 = 1$ (lower) to 4 (upper). Laser locking characteristics are shown as the red curves, with $\phi = -5\pi/6$ (upper left) to $5\pi/6$ (lower right).

When a resonator is pumped conventionally, the intracavity power P will approach its equilibrium given by Eq. (S11). In the case of feedback-locked pumping, such power changes will also have an effect on the locking response function χ, pulling the detuning to the new locking equilibrium as well (Fig. 2b,e in main text). A special case is $\phi = 0$, where the locking equilibrium can be simply described as

$$\alpha = \frac{3}{2}P \tag{S15}$$

i.e., the detuning is pulled away from the cold cavity resonance, and the effect is exactly 3/2 times what is expected from the self phase modulation. This is an averaged effect of the self phase modulation on the soliton mode and the cross phase modulation of the backscattered mode from the soliton mode. More generally, the detuning can be solved in terms of P as

$$\alpha = \frac{3}{2}P - \cot\phi + \frac{\sqrt{4 + P^2\sin^2\phi}}{2\sin\phi} \tag{S16}$$

where again only the solution satisfying $\partial\chi/\partial\alpha < 0$ is given. Neglecting the higher-order $P^2\sin^2\phi$ term inside the square root results in a lowest order approximation:

$$\alpha = \tan\frac{\phi}{2} + \frac{3}{2}P \tag{S17}$$

which splits into two additive contributions: one from the feedback phase and the other from the averaged nonlinear shift. This is Eq. (1) in the main text when written using dimensional quantities. We note that Eq. (1) in the main text uses power normalized to threshold power, while in the above analysis we used energy normalized to threshold energy. The intracavity power and energy only differ by a factor of round-trip time, and the normalized quantity is essentially the same.

When the dispersion term is considered, the CW solution is no longer stable, which leads to the formation of modulational instability (MI) combs. These combs will evolve into solitons if the CW state is also inside the multistability region of the resonator dynamics. By adjusting the pump power $|F|^2$ and feedback phase ϕ, we can change the operating point of the cavity, and map the possible comb states to a phase diagram with $|F|^2$ and ϕ as parameters (Fig. 4b in the main text). It should be noted that as soon as combs start to form inside the resonator, the CW results after Eq. (S11) become invalid (i.e., due to power appearing in the sidebands, we have $P > |\rho|^2$ when combs are formed instead of $P = |\rho|^2$ in the CW case), and such comb formation will slightly shift the operating point of the system. However, the CW results still indicate whether and how such combs can be started. Contrary to conventional pumping phase diagrams (with $|F|^2$ and α as parameters), where soliton existence regions only imply the possible formation of solitons due to multistability, the soliton existence region here guarantees the generation of solitons as the system bypasses the chaotic comb region before the onset of MI.

We have also performed numerical simulations to verify the above analyses (Fig. S2). The simulation numerically integrates Eq. (S4) with a split-step Fourier method. Noise equivalent to about one-half photon per mode is injected

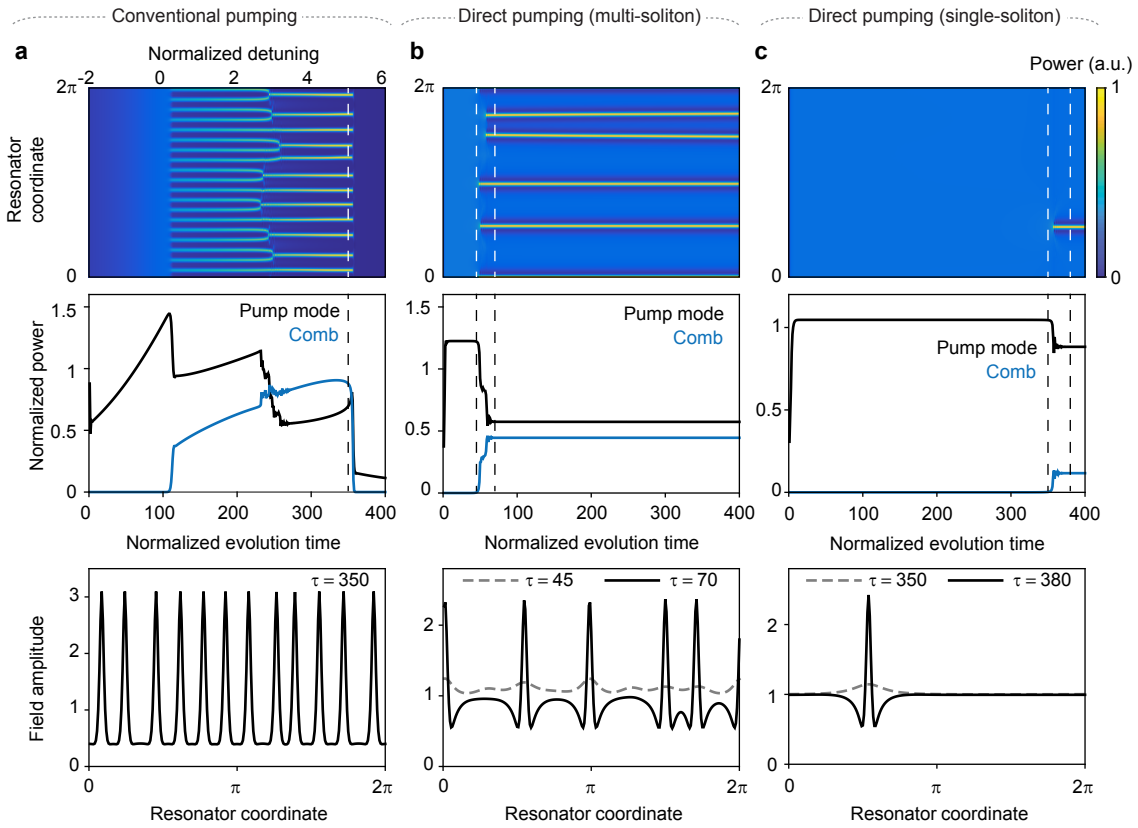

Fig. S2: **Numerical simulations of turnkey soliton generation. a**, Conventional solitons are generated by sweeping the laser frequency. Parameters are $K = 0$ (no feedback) and $|F|^2 = 4$. The normalized laser frequency is swept from $\alpha_L = -2$ to $\alpha_L = 6$ within a normalized time interval of 400. Upper panel: soliton field power distribution as a function of evolution time and coordinates. Middle panel: dynamics of the pump mode power (black) and comb power (blue). Lower panel: a snapshot of the soliton field at evolution time $\tau = 350$ ($\alpha_L = 5$), also marked as a white dashed line in the upper panel and a black dashed line in the middle panel. **b**, Multiple solitons are generated under conditions of nonlinear feedback. Parameters are $K = 15$, $\phi = 0.15\pi$, $|F|^2 = 3$ and $\alpha_L = 5$. Upper and middle panels are the same as in (a). Lower panel: snapshots of the soliton field at evolution time $\tau = 45$ (grey dashed line) and $\tau = 70$ (black solid line), also marked as white dashed lines in the upper panel and black dashed lines in the middle panel. **c**, A single soliton is generated under conditions of nonlinear feedback. Parameters are $K = 15$, $\phi = 0.3\pi$, $|F|^2 = 3$ and $\alpha_L = 5$. Upper and middle panels are the same as in (a). Lower panel: snapshots of the soliton field at evolution time $\tau = 350$ (grey dashed line) and $\tau = 380$ (black solid line), also marked as white dashed lines in the upper panel and black dashed lines in the middle panel.

into ψ to provide seeding for comb generation. Parameters common to all simulation cases are $D_2/\kappa = 0.015$ and $|\beta| = 0.5$, while others are varied across different cases and can be found in the caption of Fig. S2. As an aside, the magnitude of β was estimated from the resonant backscatter reflectivity. The resonant reflection (measured to be in the range of 4% - 20%) was measured by the detecting the reflected optical power from the resonator while scanning a laser across the resonances. In the first case (Fig. S2a), conventional soliton generation by sweeping the laser frequency is presented, showing the dynamics of a random noisy comb waveform collapsing into soliton pulses. This is in contrast to the turnkey soliton generation in the second case (Fig. S2b), where solitons directly "grow up" from ripples in the background. Such ripples are generated by MI in those sections of the resonator with local intracavity power above the threshold. Each peak in the ripples corresponds to one soliton if collisions and other events are not considered. The process of growing solitons out of the background will continue until there is no space for new solitons or when the background falls below the MI threshold, and such dynamics explain the tendency of the turnkey soliton state to consist of multiple solitons. By carefully tuning the phase and controlling the MI gain, it is still possible to obtain a turnkey single soliton state, as shown in the third case (Fig. S2c).

There are Supplementary videos that were created to illustrate the evolution processes corresponding to Fig. S2.

II. ADDITIONAL MEASUREMENTS

A. Different types of microcombs in the injection locking system

There are several interesting solutions other than stable solitons that can be derived from the regular Lugiato-Lefever equation[2]. One is the breather soliton, which is the type of soliton whose shape oscillates in time. Another example is the chaotic comb, which corresponds to the unstable Turing patterns or soliton state as the pump power is increased. In addition, solitons can be self-organized and form an equidistant pulse train in the microresonator, which is called a soliton crystal.

It is also possible to operate our system in different types of microcomb states under certain feedback phase and laser driving frequency. Fig. S3 shows the experimental spectra of breather solitons, a chaotic comb and a soliton crystal state, respectively. The turnkey generation of the chaotic comb is further shown in Fig. S4a. The broad and noisy RF spectrum indicates that it is not mode-locked.

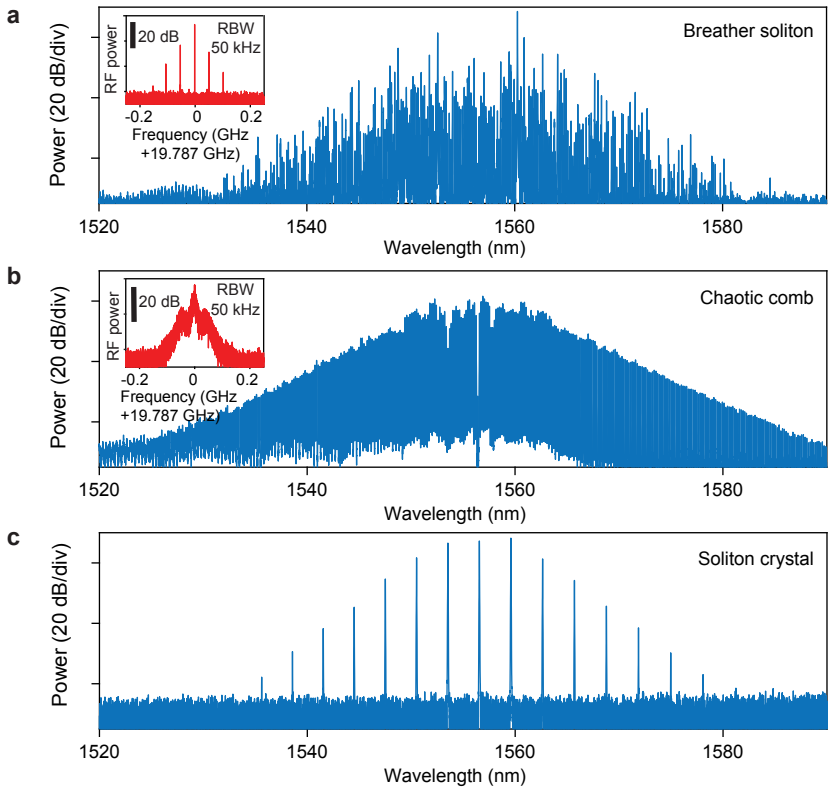

Fig. S3: **Optical and electrical spectra of different microcomb types. a**,**b**, Optical spectra of breather solitons and a chaotic comb. Inset: Electrical beatnote signals. **c**, Optical spectrum of a soliton crystal state.

B. Tuning of turnkey soliton microcomb system

To further explore the performance of the turnkey soliton microcomb system, the frequency of the pump laser is driven by a linear current scan (Fig. S4b,c). The scan speed of the driving frequency is around 0.36 GHz/ms, estimated from the wavelength-current response when the laser is free running. When the laser is scanned across the resonance, feedback locking occurs and pulls the pump laser frequency towards the resonance until the driving frequency is out of the locking band. As shown in Fig. S4b, the power steps indicate that soliton states with different soliton numbers can be accessed as we tune the driving current. It is worth noting that the soliton microcombs can be powered-on when the laser is scanned from red-detuned side (Fig. S4c), which seldom happens under conventional pumping, except in cases of an effectively negative thermo-optic response system[3]. The comb evolution during laser scanning is a useful tool to assess the robustness of the turnkey soliton generation.

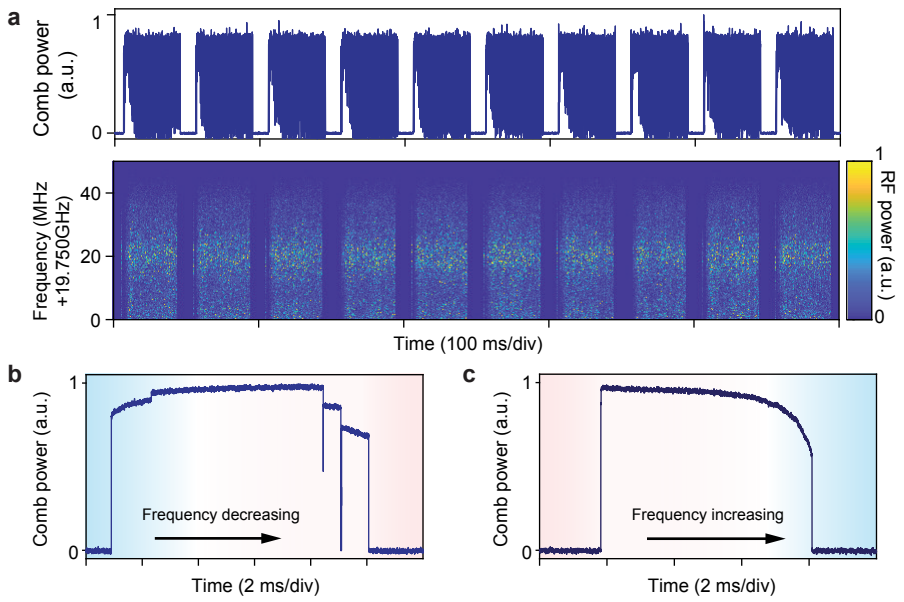

Fig. S4: **a**, Turnkey generation of a chaotic comb. Upper panel: Comb power evolution. Lower panel: Spectrograph of RF beatnote power. **b**,**c**, Comb power evolution when the pump laser frequency is driven from blue to red (**b**) and red to blue (**c**).

[1] Kondratiev, N. *et al.* Self-injection locking of a laser diode to a high-Q WGM microresonator. *Opt. Express* **25**, 28167–28178 (2017).

[2] Godey, C., Balakireva, I. V., Coillet, A. & Chembo, Y. K. Stability analysis of the spatiotemporal Lugiato-Lefever model for Kerr optical frequency combs in the anomalous and normal dispersion regimes. *Phys. Rev. A* **89**, 063814 (2014).

[3] He, Y. *et al.* Self-starting bi-chromatic $LiNbO_3$ soliton microcomb. *Optica* **6**, 1138–1144 (2019).